Studies on the photocatalysis of core-shelled SiO$_2$–Ag nanospheres by controlled surface plasmon resonance under visible light

Ko-Ying Pan[a], Yi-Fan Liang[a], Ying-Chih Pu[b], Yung-Jung Hsu[b], Jien-Wei Yeh[a], Han C. Shih[a,c,*]

[a] Department of Materials Science and Engineering, National Tsing Hua University, Hsinchu 30013, Taiwan, ROC
[b] Department of Materials Science and Engineering, National Chiao Tung University, Hsinchu 30010, Taiwan, ROC
[c] Department of Chemical and Materials Engineering, Institute of Nanomaterials, Chinese Culture University, Taipei 11114, Taiwan, ROC

ARTICLE INFO

ABSTRACT

Abundant core-shelled silica–silver nanospheres with uniform diameter and morphology were successfully synthesized by Stöber and seed-mediated method, in sequence. By the different additions of glucose, the silver nanoparticles were deposited on silica spheres by redox reaction, which well controlled in the range from 10 to 50 nm. The surface plasmon resonance absorption band shifted toward infra-red region and became broader gradually during the dimensions of silver nanoparticles were increased in the growth range. The amazing data imply that using core-shelled silica–silver nanospheres efficiently enhances the degradation of the organic pollutants under solar energy, which means the core-shelled silica–silver nanospheres is not only a cost-effective route but an energy-saving way to our planet.

© 2014 Elsevier B.V. All rights reserved.

1. Introduction

During the last decades, the photocatalyst materials have attracted substantial scientific and technological interests in biomaterials due to its potential of changing solar energy into chemical energy [1,2]. In general, many metal oxides are used as semiconductor photocatalysts, e.g., TiO$_2$ [3], ZnO [4], SnO$_2$ [5], ZrO$_2$ [6] and so on. Thanks to its good chemical stability and effective photodegradation activity for organic pollutants in air and water, TiO$_2$ is the most popular in current semiconductor photocatalysts. However, the extra light must provide the energy above 3.26 eV, which be able to trigger the TiO$_2$ electrons to conduction band from valence band, and it also means the ultraviolet light (UV light) can be only useful in this condition [7,8]. It is a challenge to overcome this limitation in the TiO$_2$ photocatalyst materials because the dominant part of solar energy is visible light not UV light in our daily life.

Fortunately, several literatures exhibit core-shelled silica–metal nanostructures consisting of silica nanocore and metal nanoshells have drawn a lot of attentions due to their special properties and applications, such as catalysts [9], SERS [10], bio-sensors [11], solar cells [12] and so on. Up to now, various routes have been explored to produce such a nanostructure, i.e., sono-chemical deposition [13], surface functionalization [14], photoreduction [15] and electroless plating [16,17]. Metal–silica core-shelled nanostructures are more stable than pure metal nanoparticles because the latter is always tending to aggregate in solution. On the other hand, the surface plasma resonance (SPR) frequency is under control easily by modifying geometries of core-shelled silica–metal nanostructures [18]. Throughout the previous papers, the resonance spectrum is related for the particle parameters as size, morphology and surrounding media, which explained via Mie scattering theory [18–21].

Base on this concept, core-shelled silica–silver nanospheres (SiO$_2$@Ag NSs) were synthesized by a step-by-step manufacture in this task. First, the silica nanospheres were prepared by Stöber method [22]. Second, silver shells were deposited on silica spheres by seed-mediated method, which means the growth of the silver seeds on silica spheres in a simple process by various additions of glucose as the reduction. In order to investigate the relations between the SPR absorbance region and photocatalyst efficiency, the authors tuned the SPR absorbance region of SiO$_2$@Ag NSs from 420 nm to 700 nm and used methylene blue (MB) as the probe to estimate the photocatalyst efficiency under visible light illuminations [23].

2. Experimental

2.1. Reagent

Eight reagents are used in this study as follows: tetraethyl orthosilicate (TEOS, 98%, Alfa Aesar), absolute ethanol (99.99%, Sigma–Aldrich), silver nitrate (99.9%, Mallinckrodt), aqueous ammonia solution (30–33%, Sigma–Aldrich), (D-(+) glucose monohydrate) (99%, Alfa Aesar), tin(II) chloride dihydrate ($SnCl_2 \cdot 2H_2O$, 98%, Sigma–Aldrich), sodium hydroxide (NaOH, 99%, Sigma–Aldrich), and methylene blue (MB, 99.9%, Sigma–Aldrich). All reagents without additional purification and Milli-Q water ($\Omega > 10^{18}$) were used in the whole procedure.

2.2. Synthesis of SiO_2 nanospheres

Silica spheres with diameter around 150 nm were prepared by well-known Stöber method with a diverse dispersion of size less than 13%. First, 3 ml TEOS and 20 ml DI-water were mixed and then the mixed solution was kept heating on the hot plate. When the temperature of mixed solution had reached 75 °C, 10 ml aqueous ammonia drops were added into this mixed solution one by one in 2 min; meanwhile, the temperature of the mixed solution was maintained at 75 °C. After the additions of aqueous ammonia drops, the solution was maintained at 75 °C for 3 h. When the reaction was done, the SiO_2 nanospheres were obtained by centrifuge at 7200 r.p.m. for 10 min. Then the products were washed 3 times by ethanol and dried in an oven at 60 °C for 5 h.

2.3. Preparation of core-shelled SiO_2–Ag nanospheres

2.3.1. Sn^{2+}-sensitized SiO_2 nanospheres

First, 0.597 g $SnCl_2 \cdot 2H_2O$ was dissolved in 50 ml HCl aqueous solution (0.01 M). The addition of HCl is to prevent the Sn(OH)Cl caused by the hydrolysis of $SnCl_2$ in the products. Second, 0.5 g as-prepared SiO_2 powders were dispersed in the above solution under ultrasonic for 30 min and then the Sn^{2+}-sensitized silica nanospheres were collected by the centrifugation and dried in the oven at 60 °C for the next step.

2.3.2. Core-shelled SiO_2–Ag nanospheres

In order to deposit silver layer on Sn^{2+}-sensitized silica nanospheres, the ammonical silver nitrate solution was first prepared as following: 0.5 g silver nitrate was added into 50 ml DI-water and then 0.2 ml NaOH (0.1 M). The color of this mixture gradually changed to yellowish-brown due to the formation of Ag_2O. Then 2 ml aqueous ammonia drops (6.6 wt%) were added into the above mixture one by one. Until the color of above solution became clear again, the $Ag(NH_3)_2^+$ solution was obtained. Next, 0.5 g Sn^{2+}-sensitized silica nanospheres were dispersed in the above ammonical silver nitrate solution under vigorous stirs. Then, after the reaction for 35 min, 1 ml glucose (10 mM) and 1 ml $Ag(NH_3)_2^+$ aqueous solution (10 mM) were added into the above solution once per 1.5 h for 4 times (1 cycle) and 8 times (2 cycles), separately. The pH of Ag deposited SiO_2 nanospheres processes was about 2–3. While the reaction was finished, the products were collected by the centrifugation and dried in the oven at 60 °C. Therefore, different morphologies and features of core-shelled SiO_2–Ag nanospheres were discovered by the three conditions (0 cycle, 1 cycle and 2 cycles). To read simply, SA0, SA1 and SA2 will be the code to represent the three conditions (0 cycle, 1 cycle and 2 cycles), respectively.

2.4. Characterizations of core-shelled SiO_2–Ag nanospheres

2.4.1. Physical analysis

The morphologies of SiO_2@Ag NSs were characterized by high resolution transmission electron microscope (HRTEM, JEM2010) and scanning electron microscope (SEM, JSM-6500F). X-ray diffraction patterns of the SiO_2@Ag NSs powder were examined by using the Shimadzu XRD6000 with CuKα radiation ($\lambda = 1.5418$ Å) scanning range (2θ) from 30° to 80°. X-ray photoelectron spectroscopy were measured at an angle of 0° using Perkin Elmer model PHI 1600 system with MgKα line as an X-ray source and the energy resolution was 1.6 eV. All the deconvolution of XPS curves were performed with the XPS Peak Fitting Program (XPSPEAK41, Chemistry, CUHK). UV–visible absorption spectra were recorded by a Hitachi U-3010 spectrophotometer.

2.4.2. Catalytic property of core-shelled SiO_2–Ag nanospheres

Each three samples of 0.5 mg SiO_2@Ag NSs were dispersed in 10 ml MB (2×10^{-5} M). In order to attach MB on three samples' surfaces, the previous solutions were under a 20-min stir, and then the solutions were exposed to a visible light source (wave length: 400–700 nm, 55 W/cm^2) for 1 h. The catalytic performances of SA0, SA1 and SA2 were recorded by monitoring the photodegardations in optical density at the fixed wavelength of the absorbance ($\lambda = 665$ nm) of the typical dye, MB, in aqueous heterogeneous solution suspensions.

3. Result and discussion

3.1. Morphologies of core-shelled SiO_2–Ag nanospheres

Fig. 1(a) shows the SEM image of silica nanoparticles with diameter about 130 nm prepared by Stöber method [22]. The silver nuclei decorated silica microspheres were manufactured by a seed-mediated method similar with electroless plating [16,17] developed by Zhu and co-workers [24]. First, a layer of Sn^{2+} was absorbed on negatively charged silica surface by electrostatic attraction, and then the $Ag(NH_3)_2^+$ were reduced immediately by Sn^{2+} through an ox-red process. From the TEM image of Fig. 1(b), after deposition of silver (SA0), the morphology was half sphere-shaped, which was getting tough and the silver nuclei on the surface of silica nanoparticles were well dispersed with the size range of 7–10 nm. Next, in order to control the morphology of silver shell, the Ag NPs were further grown with a seed-mediated method by using glucose as a mild reducing agent for 1 and 2 cycles. In the previous papers [24,25], the mixture of formaldehyde and ammonia is widely used as a reduction in a seed-mediated method, even though this combination is toxic and harmful to researchers at laboratories. Herein, a very great ideal was presented in this seed-mediated method, which was used glucose, an untoxic chemical, as a reduction. Fig. 1(c) displays the TEM image of SiO_2@Ag NSs under a 1 cycled redox reaction with glucose (SA1); the Ag NPs became larger and the diameters were about 25 nm. Fig. 1(d) demonstrated the TEM image of SiO_2@Ag NSs under a 2 cycled redox reaction with glucose (SA2); the Ag NPs are larger than previous one and the diameters were about 50 nm. All in all, judging from Fig. 1(b) to (d), the surface-modified core particles, SiO_2 nanoparticles, embedded with shell particles, Ag nanoparticles were demonstrated. Therefore, authors named these samples as core-shelled SiO_2–Ag nanospheres [26]. It was notable that the Ag NPs get larger during this growing process, they turned to be elliptic or irregular spheres and these shape conditions strongly affect the optical properties [23].
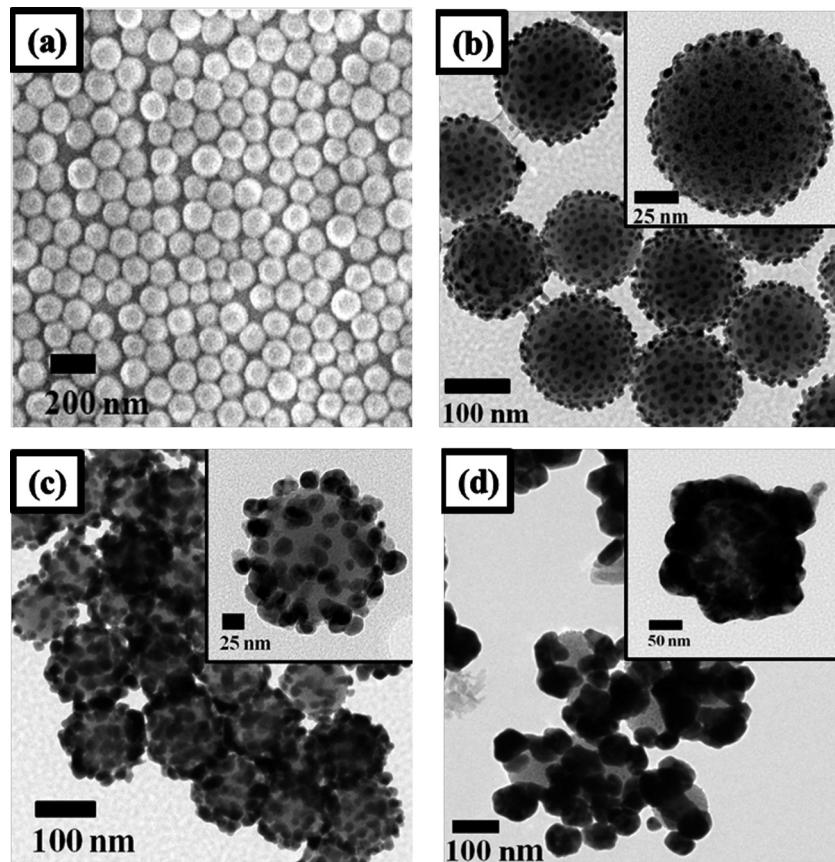
Fig. 1. (a) SEM image of silica nanospheres, (b) TEM image of SiO₂@Ag NSs (SA0), (c) TEM image of SiO₂@Ag NSs with 1-cycle redox reaction(SA1), (d) TEM image of SiO₂@Ag NSs with 2-cycle redox reaction(SA2). Upper right sides photos show the individual nanospheres TEM images taken of SA0, SA1 and SA2, respectively.

3.2. XRD pattern and HRTEM image of SiO₂@Ag

3.2.1. Nanospheres

The XRD pattern of the SiO₂@Ag composite spheres was illustrated in Fig. 2, and it exhibited peaks of 2θ angles at 37.9°, 44.1°, 64.3°, and 77.2° corresponding to the reflection of (1 1 1), (2 0 0), (2 2 0) and (3 1 1) crystalline planes in the fcc structure of typical silver. The peaks were a little broader than bulk silver because the grain size was relatively small. By calculating with Scherrer equation: $d = 0.9\lambda/B\cos\theta$ (where d is grain diameter, λ is wavelength of the X-ray = 0.1541 nm (Cu-Kα), B is full width at half max of specific peak), the grain size is about 9.8 nm of (1 1 1). To reconfirm this result, the HR-TEM image was taken in Fig. 3. The interface between one Ag NP and silica was observed and found that a Ag NP is polycrystalline with the d-spacing on it is 0.24 nm and 0.20 nm respectively, corresponding to the lattice spacing along (1 1 1) and (2 0 0) in Ag. Judging from the results of XRD and HRTEM of SiO₂@Ag NSs, the silver shells of Ag NPs were definitely pure element state, and neither oxidation state nor ionic state existed there.
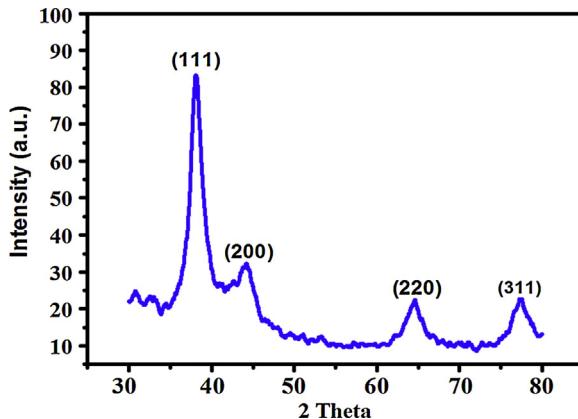

Fig. 2. XRD pattern for SiO₂@Ag NPs.
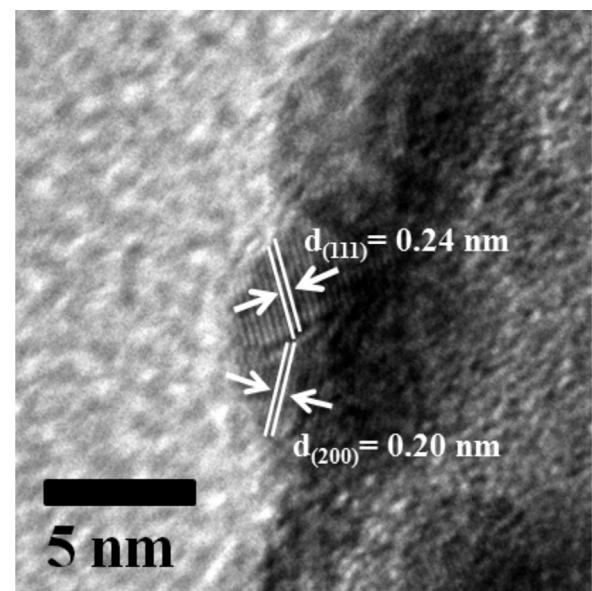

Fig. 3. HRTEM image of SiO₂@Ag NPs.
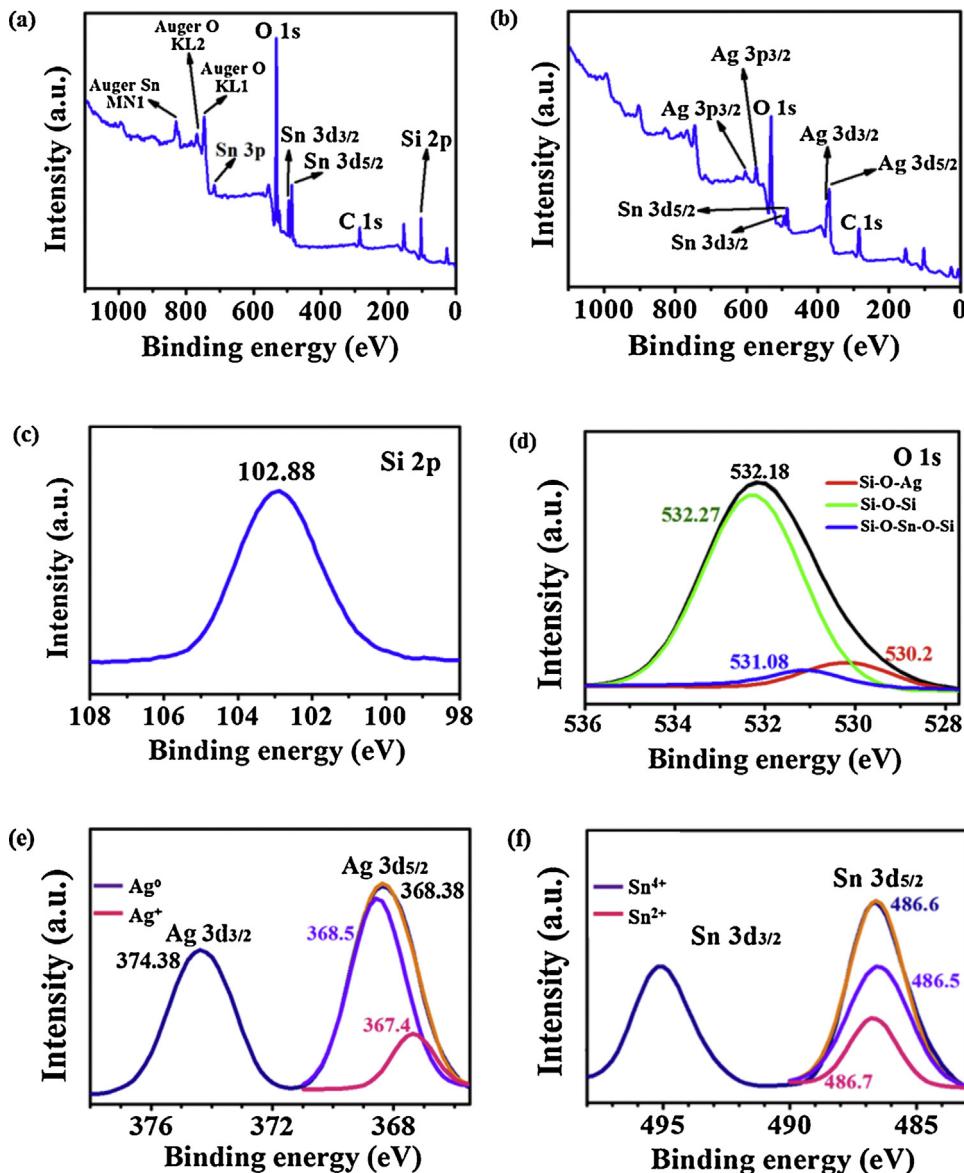
Fig. 4. The XPS of (a) survey scan of Sn^{2+}-sensitized SiO_2 nanospheres (b) survey scan of SiO_2@Ag NSs (c) Si 2p of SiO_2@Ag NSs (d) O 1s of SiO_2@Ag NSs (e) Ag 3d of SiO_2@Ag NSs (f) Sn 3d of SiO_2@Ag NSs.

3.3. XPS analysis of SiO_2@Ag nanospheres

All binding energies were referenced to the C1s line at 285.1 eV from carbon, and the spectrum deconvolutions were handled with the XPS Peak Fitting Program. The X-ray photoelectron spectroscopy for Sn^{2+}-sensitized SiO_2 nanospheres and SiO_2@Ag NSs are displayed in Fig. 4. It is obvious that after the surface of silica treated by $SnCl_2$, the new peak at around 487 eV of Sn 3d orbit could be found in Fig. 4(a). Referring to the previous paper [16] could make sure that Sn^{2+} ions absorb on the surface of SiO_2 nanoparticles in these products. Fig. 4(b) shows the representative survey of XP spectra of SiO_2@Ag NSs, and making a comparison with Fig. 4(a) could observe Ag($3d_{3/2}$, $3d_{5/2}$, $3p_{3/2}$, $3p_{1/2}$) orbits. Judging by Fig. 4(c)–(f), the binding energies of Si($2p_{3/2}$), O(1s), Ag($3d_{3/2}$), Ag($3d_{5/2}$), Sn($3d_{3/2}$) and Sn($3d_{5/2}$) are 102.88, 532.18, 374.38, 368.38, 495.20 and 486.60 eV, in sequence, which correspond closely to the previous literatures [16,25]. Mostly, Kobayashi et al. indicate that binding energies on ($3d_{5/2}$) orbit of Ag^0, Ag^+ and Ag^{2+} are 368.5, 367.6 and 367.2 eV, respectively. After the

deconvolution of O(1s) XPS curve, the binding energies of the Si—O—Ag, Si—O—Si and Si—O—Sn—O—Si unit in Fig. 4(d) are observed at 530.20, 532.27 and 531.08 eV, respectively. With referring to the previous literatures [20,25,27], the Si—O—Ag and Si—O—Sn—O—Si provide more ionic feature in the SiO_2@Ag NSs, which makes it easier to receive the core electrons from O in Si—O—Si and Si—O—Sn—O—Si more than from O in Si—O—Si. The binding energies of O in Si—O—Ag and Si—O—Sn—O—Si are much lower than that of O in Si—O—Si. Therefore, the binding energy of O(1s) in Sn^{2+}-sensitized SiO_2 nanospheres is higher than that in SiO_2@Ag nanospheres.

From Fig. 4(e), the deconvolution of Ag($3d_{5/2}$) XPS curve obtain two separated curves, which comprises one main XPS curve of Ag^0 at 368.5 eV and another one of Ag^+ at 367.4 eV. In addition, the Ag state in SiO_2@Ag NSs is Ag^0, which contains a tiny amount of $Ag(NH_3)_2^+$. In Fig. 4(f), calculating the areas under the Sn^{4+} curve and Sn^{2+} curve obtain the ratio between Sn^{4+} and Sn^{2+} on the interfaces of SiO_2@Ag nanospheres, and the ratio of Sn^{4+} to Sn^{2+} is 7:3.
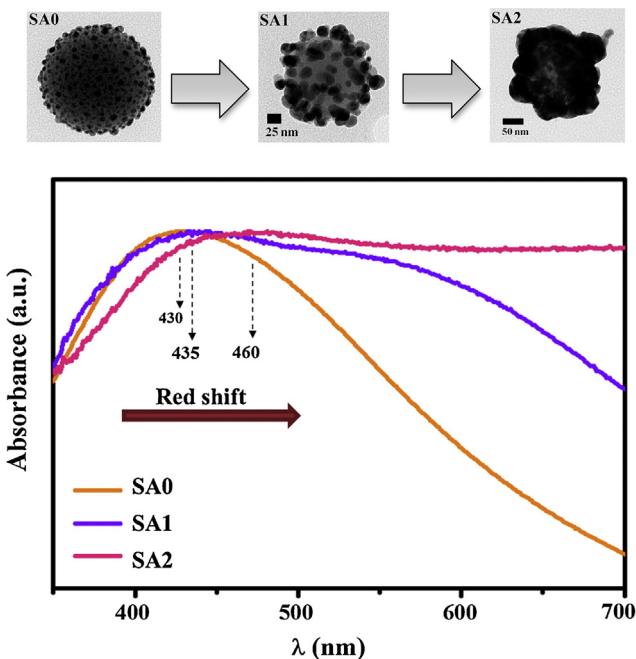
Fig. 5. UV–visible absorption spectra of three kinds of SiO$_2$@Ag NSs (SA0, SA1 and SA2).

Fig. 6. C/C_0 versus irradiation time plots for MB photodegradation.

3.4. UV–visible spectrum analysis of SiO$_2$@Ag nanospheres

As long as silver NPs are deposited on the dielectric surface of SiO$_2$ nanospheres to produce the SiO$_2$@Ag NSs successfully, the SPR characteristic of SiO$_2$@Ag NSs is always a fascinating characteristic in the optoelectronic applications. The SPR absorption of the SiO$_2$@Ag NSs can be well-aimed controlled by tuning the shell thickness of Ag as well as the core size of SiO$_2$. To understand this special optoelectronic features for SiO$_2$@Ag NSs, the SPR investigations were handled by UV–visible tests. UV–visible absorption spectra of three kinds of SiO$_2$@Ag NSs were demonstrated in Fig. 5. The UV–visible spectrum of SA0 shows an adsorption peak at 430 nm. Two absorption peaks were observed on the UV–visible spectra of SA1 and SA2, respectively. In terms of SA1, the two adsorption peaks were observed at 435 and 535 nm; for the SA2 aspect, one absorption peak was observed at 460 and another peak was observed out of 700 nm. Because the morphologies from SA0 to SA2 became elliptical increasingly, two absorption peaks were observed at SA1 and SA2 [23]. In particular, the two red shifts, one is from 430 nm, 435 nm to 460 nm; another is from 535 nm to SA2 second absorption peak in near-infrared region and broadening width of the three main absorption peaks in UV–visible spectra were observed while the dimensions of Ag NPs were grown. Eq. (1) describes the SPR shape condition κ for the two-particles system in the dipolar-coupling limit is given as [28]:

$$\kappa_{coupling} = \frac{8((s/D)+1)^3 + 1}{4((s/D)+1)^3 + 1} \tag{1}$$

where s is the interparticle surface-to-surface distance and D is the particles' size.

Eq. (2) represents the effect of the medium on the surface plasmon resonance frequency is expressed as [28]:

$$\lambda_{sp} = 2\pi c \sqrt{\frac{\varepsilon_0 m_e(\varepsilon_\infty + \kappa n_m^2)}{Ne^2}} \tag{2}$$

where κ is the same as Eq. (1), ε_0 is the permittivity of free space, m_e is the effective electron mass, ε_∞ is the high-frequency
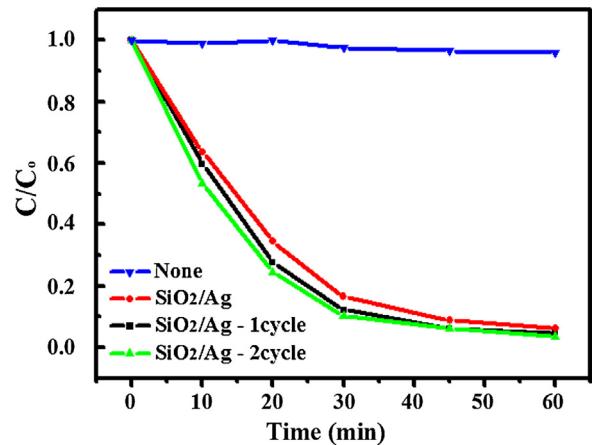
contribution to the dielectric function, n_m is the medium refractive index and N is the electron density of the metal.

The three sample preparations for UV–visible test are under the same conditions, which including the amount of nanoparticles powder, the soaked solution and the vibration time for powder separation, so s, ε_0, m_e, ε_∞, n_m and N in Eqs. (1) and (2) can be deemed to be constants. From Eq. (1), increasing D leads κ to increase near exponentially; from Eq. (2), increasing κ leads λ_{sp} to increase, too. As a result, the red shift, λ_{sp} increased, in the plasmon resonance wavelength of the coupled-system can be approximated to be proportional to the various diameters of nanoparticles. The phenomenon of Fig. 5 conforms to the result of SPR Eqs. (1) and (2), which indicates the practical applications of SiO$_2$@Ag NSs absorption band can be spanned from visible light to the near-infrared region.

3.5. Photocatalytic degradation analysis of SiO$_2$@Ag

3.5.1. Nanospheres

The SiO$_2$@Ag NSs photocatalytic degration of MB was investigated in aqueous heterogeneous liquid, as sketched in Fig. 6. C/C_0 (Y-axis) versus irradiation time (X-axis) which is recorded every 10 min for 1 h for each sample. C_0 is the initial concentration of MB and C is the MB concentration changed during the course of visible light irradiation. Three kinds of photocatalysts in aqueous heterogeneous liquid with MB, including SA0 (red line), SA1 (black line) and SA2 (green line), which be compared with the aqueous heterogeneous liquid only with MB (blue line) under the same experimental conditions, including MB density (0.5 mg/ml), the amount of photocatalysts powder, reaction time and visible light source. First, the recorded line of absent of photocatalysts proved that a slight MB degradation due to self-photolysis effect of MB molecules under visible light illumination. Second, the photocatalystic efficiency of SiO$_2$@Ag NSs was raised with increasing the size of SiO$_2$@Ag NSs. To fair compare the efficiency of SA0, SA1 and SA2, $C/C_0 = 0.1$ would be set up as a standard, and the spending time for this standard of SA0, SA1 and SA2 is 45 min, 35 min, and 30 min, respectively. Consequently, the best photocatalytic efficiency among these three samples is SA2, which indicates the photocatalytic efficiency of SiO$_2$@Ag NSs was enhanced owing to the red shift and broadening peak width of SPR absorption, as in Fig. 5. Additionally, a better photocatalytic efficiency of SiO$_2$@Ag NSs was uncovered for the core-shelled nanospheres with a larger Ag NPs size. While the absorption wave length got increasing (red shift) and SPR broadening absorption were occurred, the light-harvesting efficiency of samples was upgraded, producing plenty of charge carrier to join the MB degradation, and then MB receives

photooxidation to obtain decomposed by reacting with photogenerated holes [19,23,29].

4. Conclusion

In summary, a seed-mediated method has been successfully expanded to synthesize SiO_2@Ag NSs, and the range of Ag particle thicknesses is from 10 to 50 nm. The various reduction time and additions of glucose act a key factor in controlling the morphologies of Ag shells which coated on SiO_2 cores in these processes. Mostly, glucose is a human-friendly chemical, so making use of glucose as the reduction in electroless plating process is a great advance. In the UV–vis absorption spectrum, the noticeable red shifting and broadening of SPR characteristic absorption peak are observed, which related to the radius expansions of SiO_2@Ag NSs from 10 to 50 nm. With MB photodegradation, the present SiO_2@Ag NSs demonstrate a perfect photocatalytic quality. Moreover, adopting SiO_2@Ag NSs as catalysts in degradation under sunlight has definitely brought efficiency gains.

Acknowledgement

References

[1] N.S. Lewis, Science 315 (2007) 798.
[2] Q. Wang, J. Li, Y. Bai, X. Lu, Y. Ding, S. Yin, H. Huang, H. Ma, F. Wang, B. Su, J. Photochem. Photobiol., B 126 (2013) 47.
[3] A. Fujishima, K. Honda, Nature 238 (1972) 37.
[4] N. Kislov, J. Lahiri, H. Verma, D.Y. Goswami, E. Stefanakos, M. Batzill, Langmuir 25 (2009) 4921.
[5] L.Y. Shi, C.Z. Li, H.C. Gu, D.Y. Fang, Mater. Chem. Phys. 62 (2000) 62.
[6] T. Sreethawong, S. Ngamsinlapasathian, S. Yoshikawa, Chem. Eng. J. 228 (2013) 256.
[7] S.K. Park, K.D. Kim, H.T. Kim, Colloids Surf. A 197 (2001) 7.
[8] A. Manassero, M.L. Satuf, O.M. Alfano, Chem. Eng. J. 225 (2013) 378.
[9] S. Phadtare, A. Kumar, V.P. Vinod, C. Dash, D.V. Palaskar, M. Rpa, P.G. Shukla, S. Sivaram, M. Sastry, Chem. Mater. 15 (2003) 1944.
[10] H. Metiu, Prog. Surf. Sci. 17 (1984) 153.
[11] K.E. Shafer-Peltier, C.L. Haynes, M.R. Glucksberg, R.P. Van Duyne, J. Am. Chem. Soc. 125 (2002) 588.
[12] H.A. Atwater, A. Polman, Nat. Mater. 9 (2010) 205.
[13] H.H. Huang, X.P. Ni, G.L. Loy, C.H. Chew, K.L. Tan, F.C. Loh, J.F. Deng, G.Q. Xu, Langmuir 12 (1996) 909.
[14] I.M. Joni, R. Balgis, T. Ogi, T. Iwaki, K. Okuyuma, Colloids Surf. A 388 (2011) 49.
[15] G.N. Xu, X.L. Qiao, X.L. Qiu, J.G. Chen, Colloids Surf. A 320 (2008) 222.
[16] Y. Kobayashi, S.M. Verónica, M.L.M. Luis, Chem. Mater. 13 (2001) 1630.
[17] S. Schaefers, L. Rast, A. Stanishevsky, Mater. Lett. 60 (2006) 706.
[18] S. Linic, P. Christopher, D.B. Ingram, Nat. Mater. 10 (2011) 911.
[19] K.H. Chen, Y.C. Pu, K.D. Chang, Y.F. Liang, C.M. Liu, J.W. Yeh, H.C. Shih, Y.J. Hsu, J. Phys. Chem. C 116 (2012) 19039.
[20] M. Zhu, G. Qian, G. Ding, Z. Wang, M. Wang, Mater. Chem. Phys. 96 (2006) 489.
[21] G. Mie, Ann. Phys. 25 (1908) 377.
[22] W. Stöber, A. Fink, E. Bohn, J. Colloid Interf. Sci. 26 (1968) 62.
[23] A. Houas, H. Lachheb, M. Ksibi, E. Elaloui, C. Guillard, J.M. Hermann, Appl. Catal. B: Environ. 31 (2001) 145.
[24] M. Zhu, G. Qian, Z. Hong, Z. Wang, X. Fan, M. Wang, J. Phys. Chem. Solids 66 (2005) 748.
[25] Y.H. Kim, D.K. Lee, H.G. Cha, C.W. Kim, Y.S. Kang, J. Phys. Chem. C 111 (2007) 3629.
[26] S. Kalele, S.W. Gosavi, J. Urban, S.K. Kulkarni, Curr. Sci. 91 (2006) 1038.
[27] D.A. Pawlak, M. Ito, M. Oku, K. Shimamura, T. Fukuda, J. Phys. Chem. B 106 (2002) 504.
[28] P.K. Jain, M.A. El-Sayed, Nano Lett. 8 (2008) 4347.
[29] P. Wang, B. Huang, Y. Dai, M.H. Whangbo, Phys. Chem. Chem. Phys. 14 (2012) 9813.